Wings as inertial appendages: how bats recover from aerial stumbles

Authors: David B. Boerma[1]*, Kenneth S. Breuer [2,1], Tim L. Treskatis [3] and Sharon M. Swartz [1,2]

Author affiliations: [1]Department of Ecology and Evolutionary Biology, Brown University, Providence, RI 02912, USA. [2]School of Engineering, Brown University, Providence, RI 02912, USA. [3]Westphalian University of Applied Sciences, 45897 Gelsenkirchen, Germany.

* Author for correspondence (david_boerma@brown.edu)

Keywords:
biomechanics, flight, bats, perturbation, inertial maneuvers

Abstract

For many animals, movement through complex natural environments necessitates the evolution of mechanisms that enable recovery from unexpected perturbations. Knowledge of how flying animals contend with disruptive forces is limited, however, and is nearly nonexistent for bats, the only mammals capable of powered flight. We investigated perturbation recovery in *Carollia perspicillata* by administering a well-defined jet of compressed air, equal to 2.5 times bodyweight, which induced two types of disturbances, termed aerial stumbles: pitch-inducing body perturbations and roll-inducing wing perturbations. In both cases, bats responded primarily by adjusting extension of wing joints, and recovered pre-disturbance body orientation and left-right symmetry of wing motions over the course of only one wingbeat cycle. Bats recovered from body perturbations by symmetrically extending their wings cranially and dorsally during upstroke, and from wing perturbations by asymmetrically extending their wings throughout the recovery wingbeat. We used a simplified dynamical model to test the hypothesis that wing extension asymmetry during recovery from roll-inducing perturbations can generate inertial torques that alone are sufficient to produce the observed body reorientation. Results supported the hypothesis, and also suggested that subsequent restoration of symmetrical wing extension helped decelerate recovery rotation via passive aerodynamic mechanisms. During recovery, humeral elevation/depression remained largely unchanged while bats adjusted wing extension at the elbow and wrist, suggesting a proximo-distal gradient in the neuromechanical control of the wing.

Introduction

In nature, all flying animals contend with disruptive forces, including turbulence, wind gusts, and in-flight collisions. These perturbations interrupt symmetrical, rhythmic limb motion and impose rapid changes in body orientation. The capacity to recover from these "aerial stumbles" is necessary for flight in natural environments, but strategies for restoring control likely differ across taxa depending on the strength and type of perturbation, as well as the morphology of the wings. Recovery dynamics are therefore a critical area of study for those interested in the evolution and biomechanics of flight and in principles of motor control.

Recent work has described responses to perturbations in a few species of insects and birds. For example, dipterans and bees recover from instantaneous changes to body orientation by asymmetrically altering left vs. right wing stroke amplitude, wing stroke angle,

and/or angle of attack (Beatus et al., 2015; Ristroph et al., 2010; Vance et al., 2013). Hummingbirds maintain stability within the unsteady vortices of a von Kármán vortex street by varying wingbeat frequency, intermittently fanning the tail, and asymmetrically increasing stroke amplitude and stroke plane angle (Ortega-Jimenez et al., 2014; Ravi et al., 2015).

Flight in bats differs from that in other taxa in some fundamental ways. In particular, many bats use substantial flexion at numerous joints to fold their wings as an integral aspect of wingbeat kinematics, especially during upstroke (Håkansson et al., 2015; Iriarte-Diaz et al., 2011; Riskin et al., 2012; Riskin et al., 2010; Riskin et al., 2008; Vejdani et al., 2019), which contrasts with the relatively extended wing postures that insects and hummingbirds maintain during flight (Altshuler et al., 2010; Dudley, 2018; Kruyt et al., 2014; Warrick et al., 2005; Weis-Fogh, 1973). In bats, the highly articulated wing skeleton enables substantial wing flexion during upstroke, and most of these degrees of freedom are directly actuated by muscles in the forelimb (Bahlman et al., 2016). Indeed, the jointed skeleton of bat wings confers a high degree of control over not only wing shape and projected area, but also on the distribution of wing mass, and therefore over the wing's instantaneous moment of inertia. Bats use this aspect of their morphology when reorienting their bodies to land head-under-heels; landing maneuvers do not rely primarily on aerodynamic forces, but rather on inertial torques generated by the relatively heavy articulated wings (Bergou et al., 2015; Riskin et al., 2009). By selectively retracting one wing during portions of landing wingbeats, bats redistribute wing mass to produce net inertial moments which alone are sufficient to rapidly rotate the body to achieve landing posture and position.

We hypothesize that inertial reorientation is not restricted to landing maneuvers in bats but is also a key mechanism for other aspects of control over body orientation. Specifically, we predict that bats deploy their wings as inertial appendages to reorient their bodies during recovery from aerial stumbles. Here, we test this hypothesis by analyzing wingbeat kinematics following pitch- and roll-inducing perturbations to flights of *Carollia perspicillata*, a small fruit-eating bat, and probe the mechanisms underlying perturbation response using a computational dynamical model. We predict that bats redistribute wing mass (i) symmetrically, cranial or caudal to the center of mass, to recover from pitch-inducing perturbations; (ii) asymmetrically, mediolaterally about the center of mass, to recover from roll-inducing perturbations; and (iii) to produce inertial torques of sufficient magnitude to effect recovery rotations.

Methods

Animals and training

Study subjects were captive-bred *Carollia perspicillata*, an echolocating bat species that roosts in large groups and forages in cluttered forests (Cloutier and Thomas, 1992); during group flight and navigating foliage, they may encounter turbulence, gusts of wind, and collisions. We trained four adult males (body mass = 17.75 ± 1.24 g, mean ± s.d.) to fly the length of a flight corridor (2 m x 2 m x 8.8 m) through an adjustable window that constrained their flight path to the region below a perturbation air jet (Fig. 1A). We made conscious efforts to reduce training effects by administering perturbations randomly. All experiments and animal husbandry were approved by the Brown University IACUC and complied with USDA regulations.

Perturbation apparatus

We initiated aerial stumbles using a short-duration jet of compressed air (1.93 MPa/28 psi, 500 ms) to perturb the dorsal aspect of the body or one wing (Fig. 1B,C). The perturbation apparatus comprised a fast-switching solenoid valve (Festo MHJ-10, Festo AG & Co. KG, Germany) with an output diameter of 3.175 mm. During experiments, the tip of the valve output nozzle was approximately 7.5 cm from the bat at the onset of perturbation. We measured the force of the air jet using a flat force plate positioned below the valve, mimicking the position and orientation of the bat's body and outstretched wings relative to the air jet in our experiments. At distances of 5, 7.5, and 10 cm from the plate, the force of the compressed air jet is approximately 0.5 Newtons (~2.5 bodyweights) and can be approximated as constant during the 500 ms duration (Fig. S1). Each bat triggered its own perturbation by interrupting the beam of a laser trigger (StopShot Crossbeam Kit, Cognisys Inc., USA) just prior to flying through the window.

Motion tracking and body-referenced coordinate system

We recorded the perturbation and subsequent 3±1 wingbeats using a synchronized array of six high speed cameras (four Phantom Miro 340 cameras, Vision Research Inc., USA; plus two Photron Fastcam 1024 PCI cameras, Photron USA Inc., USA; 800 Hz framerate; 100-500 µs exposure). We used nontoxic white paint to mark 24 anatomical landmarks on the wings and body (Fig. 2A). When necessary, we anesthetized bats using isoflurane (induction via mask at 2-2.5%, then maintained at 1-1.5%; 0.8 L/min O_2 throughout the procedure) during marker application (approximately 5 minutes), and allowed

bats to recover for twenty minutes, or until they readily took food and voluntarily flew in a normal fashion, at typical speeds, within the flight corridor. We obtained 3D coordinates for each landmark using the open-source motion tracking software XMALab (Knörlein et al., 2016), and filtered the time-series positional data using a 2nd-order low-pass Butterworth filter with a cutoff frequency of 100 Hz, approximately ten times the wingbeat frequency. We measured body rotations and wing movements after transforming these 3D coordinates to a body-referenced coordinate system [X_B,Y_B,Z_B] (Fig. 2B), with the midpoint between the shoulders at [0, 0, 0]. X_B was a vector from the lumbar marker (*k* in Fig. 2A) to the inter-shoulder point (positive = cranial), Z_B was orthogonal to X_B and a vector from the right to the left shoulder (positive = dorsal), and Y_B was orthogonal to X_B and Z_B (positive = lateral, toward the bat's left).

Definitions of kinematic measurements

We report the bat's time-varying body orientation in terms of yaw, pitch, and roll angles, which we calculated using the Euler rotation sequence required to align the global coordinate system [X_G,Y_G,Z_G] with the body-referenced coordinate system [X_B,Y_B,Z_B]. We computed these angles in the traditional order of yaw, pitch, then roll (Stengel, 2015). +Y_G is horizontal within the plane of the partition window, pointing to the bat's left; +Z_G is aligned with gravity, pointing upward; and X_G is orthogonal to Y_G and Z_G, pointing forward, toward the end of the flight corridor (Fig. 1A). Note that in this coordinate system, nose-down pitching is positive. For more intuitive visual interpretation, we multiplied pitch angles by -1 following computation, so that positive values reflect rotations which elevate the nose relative to the feet.

We measured humeral elevation/depression as dorsoventral motion of the elbow relative to the shoulder. This variable is directly related to forces produced by contraction of the primary downstroke muscle, the pectoralis, and of the dorsal shoulder musculature that effects upstroke (Hermanson and Altenbach, 1985; Konow et al., 2017), and thus should directly reflect motor control of the shoulder joint. We used this angle to define wing stroke amplitude and duration. Similarly, we used humeral motion to define wing protraction/retraction, i.e. cranial/caudal sweep. We measured total wing extension as the 3D distance from shoulder to wingtip, normalized to average maximum extension, and also separately measured specific contributions to wing extension by elbow and wrist extension. We estimated angle of attack for each wing as the angle between the plagiopatagium or armwing surface (defined as the plane formed by the shoulder, tip of fifth digit, and wrist),

and the effective air velocity, given by the velocity of the wrist in [X_G,Y_G,Z_G] (Table 1) (Hubel et al., 2016). We computed left-right asymmetry for each kinematic variable as the absolute difference between the left and right wings at each time-step such that values of zero would indicate perfect symmetry between the left and right wings.

Computational model simulations

We used a simplified dynamical model of a bat to assess the relative contributions of aerodynamic and inertial forces produced by the wings to body roll, including those that enable recovery from wing perturbations (Bergou et al., 2015; Vejdani et al., 2017). This model consisted of a body and two rectangular wings that match the size, mass, and mass distribution of those of *C. perspicillata.* The wings possessed four degrees of freedom: elevation/depression, protraction/retraction, pronation/supination, and flexion/extension. The model approximated aerodynamic forces using a quasi-steady drag model (see Bergou et al. (2015) for details). Because the model's pitching dynamics are very sensitive to changes in sweep angle and wing folding, we chose to simulate only perturbations in which bats modulated wing extension to effect body roll. We modeled two roll-inducing wing perturbation trials from one individual, representing two extremes: one low (47º) and one high roll magnitude (93º) trial. We fit a high-order polynomial to the wing extension measurements for each trial, and used the resulting functions, which are descriptors of wing extension, and a function defining wing elevation/depression, as inputs to the model. From these values of wing extension over time, the model estimated body roll due to inertia alone and body roll due to inertial plus aerodynamic forces.

Trial selection and statistics

The timing of perturbation onset with respect to the wingbeat cycle and the anatomical location affected by the perturbation varied among trials and individuals, resulting in a spectrum of perturbations and responses. However, general categories of bat–perturbation interactions arose, including perturbations that affected the dorsal body midline, inducing body pitch, and those that affected one wing, inducing body roll, among others not discussed further here. We visually determined the time of perturbation onset and the affected location from the high speed videos, noting the moment at which the wing membrane or body pelage deformed from the force of the air jet and the region where this deformation occurred. We also aligned a laser pointer with the perturbation apparatus so that it would mark the affected region, providing a secondary reference for the location affected by the perturbation.

From a total of 102 perturbed flights, we selected sets of similar trials (comparable perturbation onset with respect to the wingbeat cycle, consistent anatomical location affected) for perturbations to the body (n = six trials, four individuals) and wing (n = five trials, two individuals) (Movies S1-S3). A disadvantage of this approach was that it limited our sample size to only those trials which were directly comparable. However, our choice to compare similar perturbation trials allowed us to identify consistent patterns of altered wingbeat kinematics in response to similar disturbances, and to test the specific hypothesis that these consistent kinematic responses produced inertial torques that contribute to recovering pre-disturbance body orientation. This strategy allowed us to glean first insights into the mechanistic basis for how bats recover from perturbations to body orientation,

We performed all statistical analysis in R (v. 3.4.0) (R Core Team, 2018). We compared kinematic measurements between perturbed and control measurements using linear mixed-effects models treating individual as a random effect, implemented with the *lme4* package (Bates et al., 2015). We then conducted a Tukey's all-pair comparisons post-hoc test, implemented with the *multcomp* package (Hothorn et al., 2008). We tested for differences over time in increments of 10 % of the wingbeat cycle. We used a Welch two-sample t-test to compare peak rotations between perturbed and unperturbed flights. Unless stated otherwise, we present average values as means ± 1 s.d.

Results

Recovery from pitch-inducing body perturbations

Perturbations to the dorsal midline of the body during downstroke, caudal to the center of mass, induced head-up body pitch, which peaked at 33.24º ± 15.13º, 20.74º more than average control pitch (Welch two sample t-test; t = 3.03; df = 6.91; p = 0.0097) (Figs 3A, S3). Peak pitch coincided with the end of the perturbation, at approximately the end of downstroke; therefore, the recovery began with upstroke. Within one wingbeat cycle (upstroke then downstroke), bats decreased pitch angle to near or slightly below control values.

During recovery, bats moved left and right wings symmetrically (Fig. 3B-M; wingbeats 1.5-3; Fig. S3). They extended both wings during the recovery upstroke, a period over which these bats retracted their wings in control flights (Fig. 3F-G) (Tukey post-hoc comparison; wingbeats 1.6, 1.8, and 1.9; z = -2.538, 3.025, and 9.752, respectively; p = 0.0362, 0.00837, and <0.001 respectively), primarily by unfolding the handwing via

increasing wrist extension, rather than by increasing elbow extension or humeral protraction (Fig. 3D-K; wingbeats 1.5-2). Bats completed recovery by initiating a downstroke with the humerus more retracted than when not perturbed.

Recovery from roll-inducing wing perturbations

During roll-inducing wing perturbations, the perturbation jet applied force lateral to the center of mass, to the dorsal aspect of one wing only. The perturbation began halfway through upstroke and concluded between slightly before and quarter-way through the first downstroke. These perturbations induced body roll toward the perturbed side, which peaked at 60.86º ± 22.22º, 52.05º higher than in unperturbed flights (Welch two sample t-test; t = 5.6842; df = 7.9095; p = 0.000241) (Fig. 4A). Peak roll occurred partway through downstroke, and began to decrease immediately thereafter. Therefore, this first downstroke is the recovery downstroke. Within one wingbeat cycle (downstroke then upstroke), bats decreased roll angle to baseline values (Fig. 4A).

The primary kinematic response to wing perturbations during the recovery wingbeat was to adjust left and right wing extension asymmetrically while flapping, especially during the portion of recovery downstroke which coincides with decreasing roll values (Figs 4F-G, S4) (total left-right asymmetry during wingbeats 1.4 and 1.5, perturbed vs. unperturbed: Tukey post-hoc comparison; z = 2.409 and 2.319 respectively; p = 0.0371 and 0.0467 respectively). During the recovery downstroke (wingbeats 1.25-1.5), they selectively retracted the unperturbed wing while extending the perturbed wing via elbow and wrist extension. Bats also decreased angle of attack on the unperturbed side compared to control values during recovery downstroke (Fig. 4L-M) (Tukey post-hoc comparison; wingbeats 1.3, 1.4, and 1.5; z = -2.760, -2.5789, and -3.564, respectively; p = 0.0197, 0.0351, and 0.00117 respectively). During the recovery upstroke, bats reversed the side of wing extension and angle of attack asymmetry by selectively extending the wing on the unperturbed side compared to control values (Tukey post-hoc comparison; wingbeats 1.6, 1.7, and 1.9; z = -4.057, -2.5998, and <0.001 respectively; p = <0.001, 0.0308, and 0.0001 respectively) while also decreasing its angle of attack (Tukey post-hoc comparison; wingbeat 1.6; z = -2.822; p = 0.017).

Computational model simulations

We used the dynamical model to simulate two specific wing perturbation trials from the same individual, where peak perturbed body roll orientation was 47º (low roll magnitude case) and 93º (high roll magnitude case) respectively. These trials represent the extremes observed over all recorded flights. Model outputs for each case revealed that inertial torques generated by flapping asymmetrically-extended wings were sufficient to produce substantial body roll (Fig. 5C and G, green lines). However, in the high roll magnitude case the addition of fluid (aerodynamic) forces was required to accomplish the deceleration observed in recovery rotation (Fig. 5C and G, purple lines). Additionally, as the magnitude of left-right asymmetry in wing extension increases (Fig. 5B vs. F), so too does the resulting body roll (Fig. 5C vs G).

Discussion

Perturbations produced two types of aerial stumbles, depending on where the air jet applied force. Body perturbations occurred when a downward jet of compressed air impacted the posterior dorsal body midline, which led to a head-up pitched orientation while the wings continued to flap symmetrically (Figs 1C, 3, S3). Perturbations directly to the dorsal aspect of one wing induced body roll toward the affected side and prompted brief left-right kinematic asymmetry (Figs 1B, 4, S4). Bats recovered from each type of aerial stumble by initiating rotation in the direction opposite to that imposed by the perturbation, then decelerating this rotation as they approached a stable body orientation (i.e. horizontal). The net torques on the body that produced these recovery rotations arose from altered wing movements during the recovery wingbeat, and depending on the dominant kind of rotation, pitch vs. roll, each type of recovery carried a particular kinematic signature that allowed the bats to restore stable, horizontal flight within only one wingbeat.

Mechanisms of recovery

Recovery from pitch-inducing body perturbations was marked by symmetrical wing extension during the recovery upstroke, a period in the wingbeat cycle during which *C. perspicillata* and other bat species usually fold the wings (Fig. 3F, wingbeat 1.5-2.0). By extending the wings anterior to the center of mass while elevating them during upstroke, *C. perspicillata* propels its wing mass forward and upward relative to the body, which, due to the conservation of angular momentum, could produce an inertial torque that pitches the body ventrally (head-down). This prediction could be tested with a dynamical model simulation.

However, unlike simulating rolling maneuvers, which is quite robust to input parameters, simulating pitching maneuvers with the minimal model described above has been shown to be unreliable as the results are very sensitive to small details in the animal morphology and flapping kinematics. Flapping flight in insects is very unstable in pitch (e.g. Sun et al., 2007), and Bergou et al. (2015) show that a bat's flight simulated using the model employed in this study can exhibit either positive or negative pitching behavior depending on subtle shifts in the relative size of the inertial and aerodynamic coefficients, as well as on small changes in the degree of wing folding. In the absence of a higher fidelity simulation model that uses measurements capturing the full complexity of the wing motion (see also Bergou et al., 2015), efforts to model pitching recovery maneuvers are beyond the scope of this study.

Bats recovered from roll-inducing wing perturbations using a two-step response. First, they initiated recovery body roll with an inertial impulse via asymmetrical wing extension (Fig. 4F-G). Our computational model shows that the inertial impulse alone generates enough torque to roll the body into a recovered orientation within one wingbeat (Fig. 5C and G, green curves), and that the magnitude of the inertial impulse tracks the extent of left-right asymmetry in wing extension (Fig. 5A-D vs. E-H, green curves). In the second step, bats suppressed this rotation once symmetrical wing extension was restored. Above a certain threshold of body roll this rotational damping may be aerodynamic, and arise passively from net asymmetry in wing velocity relative to the air as the bats flap while rotating, by the phenomenon known as flapping counter-torque (Hedrick et al., 2009). Our model provides support for this interpretation in the high roll magnitude case (93º), because the rate and magnitude of body roll decreases once left-right symmetry is restored, but only when the model includes aerodynamic effects (Fig. 5G, purple curve, x=~1.75 wingbeats). These model results thus support our hypothesis that bats use wing inertia to control body orientation in a variety of scenarios, including recovery from aerial stumbles as well as in landing maneuvers, as we have shown previously (Bergou et al., 2015).

Evolutionary perspectives and hypotheses regarding the neural control of flight in bats

Consideration of the evolutionary history of form and function can help guide interpretations of behavior and morphology in extant taxa and provides a framework for generating new hypotheses. The relatively heavy, jointed architecture that now comprises the bat wing skeleton originally evolved for terrestrial locomotion in non-volant bat ancestors (Bishop, 2008; Curet et al., 2012; Gunnell and Simmons, 2012; Simmons et al., 2008), and has since been coopted for its current role in defining and controlling wing shape and wing

motion during flight. An obvious effect of the bat limb skeleton's ability to define, move, and shape the wing is the capacity to produce the aerodynamic forces that enable powered flight. However, recent work, including the present study, is beginning to show that the emergent inertial properties of heavy, jointed wings in bats have also been coopted to produce inertial torques that reorient the body during ecologically critical maneuvers, such as landings (Bergou et al., 2015) and recovery from flight disturbances. As evidence of the latter, we demonstrate that bats unilaterally adjust joint angles at the elbow and wrist during recovery from roll-inducing perturbations. These movements retract one wing relative to the other, thus introducing left-right asymmetry in the wing moments of inertia. Our dynamical model shows, through simulation, that inertial torques that arise from this asymmetry are sufficient to produce body roll on the order of that observed in many experimental trials, but that body roll above a certain threshold requires that wings function as both inertial and aerodynamic structures. Perturbation recovery for bats is thus an inertial as well as an aerodynamic maneuver.

It may be surprising that inertial effects could be useful for a flying organism because in such animals, evolution tends to select for weight reduction, particularly in the wings. Indeed, the relative mass of the bat wing skeleton has prompted kinematic strategies (Riskin et al., 2012; Vejdani et al., 2019) and morphological and material modifications (Swartz, 1997; Swartz and Middleton, 2008; Vaughan, 1959; Vaughan, 1970a; Walton and Walton, 1970) that mitigate the inertial cost of flapping heavy, jointed wings. Bats therefore appear to strike a balance between mitigating the inertial cost of flight while also deploying the wings as inertial appendages during instances that require rapid body reorientation. Gould and Vrba (1982) provide a relevant term, "exaptations," which they define as "characters, evolved for other uses (or for no function at all), and later 'coopted' for their current role." We thus interpret the jointed musculoskeletal anatomy of bat wings as an exaptation for flight, which produces not only aerodynamic but also inertial effects that both contribute to stable and agile movement through an aerial environment.

In the same way that an ancestral terrestrial condition for limb morphology was later coopted into the bat wing, we predict that aspects of ancestral terrestrial motor control may not only be retained into the extant bat lineage but might also provide functional advantages for bats recovering from aerial stumbles. Our experiments did not include measurement of muscle activity which would be required to directly test this prediction, but our kinematic results allow us to pose hypotheses about the underlying motor control patterns that may have

produced the motion that we measured. We include the following discussion to more fully articulate these hypotheses and guide future investigations into the neural control of flight.

Perturbation experiments that integrate measurements of limb motion, muscle activity, and neural control, are an effective and well-established tool for gaining improved understanding of the neuromechanics of locomotion (Daley and Biewener, 2006; Dickinson et al., 2000; Jindrich and Full, 2002; Nishikawa et al., 2007; Ristroph et al., 2010; Sponberg and Full, 2008; Vance et al., 2013). Recent work in this field has uncovered a link between a proximo-distal gradient in muscle-tendon architecture in terrestrial tetrapod limbs and a corresponding gradient in neuromechanical control (Biewener and Daley, 2007; Daley et al., 2007). Proximal muscles (e.g. pectoralis and dorsal shoulder musculature in the forelimb or the hamstring and quadriceps complexes in the hindlimb) tend to be parallel-fibered and have short tendons. They thus directly actuate motion at proximal joints and are mechanically insensitive to perturbations. In contrast, many distal muscles (e.g. biceps, triceps, and wrist flexors/extensors in the forelimb or the gastrocnemius and digit flexors in the hindlimb) are pennate-fibered, multiarticular, and possess relatively long tendons. In some cases, when distal muscles with this morphology contract, rather than transferring contractile force directly to the skeleton and thus producing movement at the limb joints, this force can be stored as elastic energy in the long, gracile tendons (Alexander and Bennet-Clark, 1977; Roberts and Azizi, 2011). Joint motion then proceeds only once the tendon begins to recoil, thus decoupling the timing of muscle contraction from the onset of joint motion. These intrinsic muscle-tendon properties passively adjust the motion of distal joints in response to altered limb loading during perturbed strides along with active modulation in motor patterns according to afferent neural feedback (Daley and Biewener, 2011; Daley and Biewener, 2006).

During the evolution of flapping flight, bats retained not only a jointed forelimb skeleton but also this ancestral gradient in limb muscle architecture (Vaughan, 1970b). We thus hypothesize that they employ a similar neuromechanical control gradient and suggest that future work seek to test this hypothesis using electromyography (EMG) to directly measure the neural inputs to key flight muscles that generate motion at the shoulder, elbow, and wrist during recovery from aerial stumbles. Our kinematic measurements suggest that bats might alter motor patterns along a proximo-distal gradient in ways that are consistent with findings for terrestrial bipeds and quadrupeds. Humeral elevation/depression (motion at the proximal joint) is not significantly different from unperturbed flight during recovery wingbeats. This stands in contrast to significant changes in flexion/extension at the more

distal elbow and wrist that can be symmetrical or asymmetrical depending on the rotational axis of recovery. We predict motor pattern conservation for the pectoralis and dorsal upstroke musculature to maintain cyclic wingbeats, and modulation of activity of muscles that control the distal joints in response to perturbations. Altered patterns of motion at the elbow and wrist following perturbation could arise from changes in activation patterns for flexor and extensor muscles, such as the biceps brachii, triceps brachii, extensor carpi radialis longus (ECRL) and flexor digitorum profundus (FDP) alone, or some more complex combination of muscle action and tendon elastic recoil (Konow et al., 2015). Changes to motoneuronal firing patterns could be initiated by afferent feedback from proprioceptors within distal muscles in a manner similar to that observed in the hindlimb muscles in tetrapods (Donelan and Pearson, 2004; Gorassini et al., 1994; Hiebert et al., 1994).

Suggestions for future work and conclusions

Although we have examined only one form of perturbation in the present study (a dorsal air jet focused on a specific portion of the wing or body), the ultimate result of this disruption is a rapid change in body orientation. This is an effect that many natural disturbances can produce, including large-scale gusts, turbulence, and collisions of bats with conspecifics, other animals, and objects in the physical environment. We predict that the details of kinematic responses to other perturbations will differ from those described in this study, and that future work will identify additional recovery strategies that may be specific to other types of perturbations. However, we anticipate that inertial mechanisms will be broadly important for controlling body orientation in diverse scenarios and that our interpretation of the relatively heavy, highly jointed morphology of bat wings as an exaptation for flight with the propensity to function as inertial appendages will remain consistent with future findings. We hope that the present study will serve as a starting point for future investigations into how bats respond to unsteady conditions, particularly responses to continuous turbulent flows, such as a von Kármán vortex street, and responses to broad-scale atmospheric turbulence, such as up- and downdrafts. We also suggest that flight perturbation studies, particularly those that focus on bats, seek to include measurements of muscle activity in the target muscles outlined in the preceding section. Such experiments would shed light on the neural control of flight and would provide insight into how ancestral motor control paradigms may or may not be conserved alongside the morphology of the flight apparatus.

In summary, this study presents the first insights into how bats recover from disturbances to body orientation during flight and demonstrates that individuals recovered pre-disturbance body orientation within one wingbeat following air jet perturbations of 2.5 times their bodyweight. This recovery time was consistent across two types of perturbations: those that induced body pitch and those that induced body roll. In each case, bats responded primarily by modulating wing extension; however, this response was bilaterally symmetric during recovery from pitch-inducing perturbations, whereas it was bilaterally asymmetric during recovery from roll-inducing perturbations. Dynamical modeling showed that the asymmetrical response generated inertial torques that were sufficient to produce the observed recovery body roll, and that in cases of high magnitude body roll aerodynamic damping was necessary to decelerate the recovery rotation.

These results highlight that remnants of the ancestral mammalian forelimb, namely the retention of the numerous bones, muscles, and articulations in the wing, invest the wings with the ability to control body orientation as inertial appendages during recovery from aerial stumbles. Our findings raise interesting questions about the evolution of neural control for flight as bats transitioned from terrestrial ancestors, and we suggest that future research seek to explore how the proximo-distal control paradigm of terrestrial tetrapods is manifest in the control of bat wings.

Acknowledgements. Many thanks to Phillip Lai for providing figures for modification; to Caleb Anderson, Okuoma Idah, Molly Magid, Max Quinn, and Melissa Sierra, for digitizing anatomical landmarks by hand; to Erika Tavares and the Brown University Animal Care staff for their assistance with animal husbandry; to Hamid Vejdani for assistance with the dynamical model; and to members of the Morphology Group at Brown University for enriching conversation and patience that has helped shape this work.

Competing interests. The authors declare no competing or financial interests.

Funding. This research was supported by NSF grant CMMI 1426338 and Air Force Office of Scientific Research (FA9550-12-1- 0301), monitored by P. Bradshaw.

Data Availability. The data supporting this article are available from the Brown Digital Repository: https://doi.org/10.26300/t0wd-8q84

Literature Cited

Alexander, R. M. and Bennet-Clark H. C. (1977). Storage of Elastic Strain Energy in Muscle and Other Tissues. *Nature.* **265**, 114–117.

Altshuler, D. L., Dudley, R., Heredia, S. M. and McGuire, J. A. (2010). Allometry of hummingbird lifting performance. *J. Exp. Biol.* **213**, 725–734.

Bahlman, J. W., Price-Waldman, R. M., Lippe, H. W., Breuer, K. S. and Swartz, S. M. (2016). Simplifying a wing: diversity and functional consequences of digital joint reduction in bat wings. *J. Anat.* **229**, 114–127.

Bates, D., Mächler, M., Bolker, B. and Walker, S. (2015). Fitting Linear Mixed-Effects Models Using lme4. *J. Stat. Soft.* **67**, 1–48.

Beatus, T., Guckenheimer, J. M. and Cohen, I. (2015). Controlling roll perturbations in fruit flies. *J. R. Soc. Interface.* **12**, 20150075–20150075.

Bergou, A. J., Swartz, S. M., Vejdani, H., Riskin, D. K., Reimnitz, L., Taubin, G. and Breuer, K. S. (2015). Falling with style: Bats perform complex aerial rotations by adjusting wing inertia. *PLoS Biol.* **13**, e1002297.

Biewener, A. A. and Daley, M. A. (2007). Unsteady locomotion: integrating muscle function with whole body dynamics and neuromuscular control. *J. Exp. Biol.* **210**, 2949–2960.

Bishop, K. L. (2008). The evolution of flight in bats: narrowing the field of plausible hypotheses. *Q. Rev. Biol.* **83**, 153–169.

Cloutier, D. and Thomas, D. W. (1992). *Carollia perspicillata*. *Mammalian Species.* 1–9.

Curet, O. M., Swartz, S. M. and Breuer, K. S. (2012). An aeroelastic instability provides a possible basis for the transition from gliding to flapping flight. *J. R. Soc. Interface.* **10**, 20120940–20120940.

Daley, M. A. and Biewener, A. A. (2011). Leg muscles that mediate stability: mechanics and control of two distal extensor muscles during obstacle negotiation in the guinea fowl. *Philos. Trans. R. Soc. Lond., B, Biol. Sci.* **366**, 1580–1591.

Daley, M. A. and Biewener, A. A. (2006). Running over rough terrain reveals limb control for intrinsic stability. *Proc. Natl. Acad. Sci. U.S.A.* **103**, 15681–15686.

Daley, M. A., Felix, G. and Biewener, A. A. (2007). Running stability is enhanced by a proximo-distal gradient in joint neuromechanical control. *J. Exp. Biol.* **210**, 732–732.

Dickinson, M. H., Farley, C. T., Full, R. J., Koehl, M. A., Kram, R. and Lehman, S. (2000). How animals move: an integrative view. *Science.* **288**, 100–106.

Donelan, J. M. and Pearson, K. G. (2004). Contribution of Force Feedback to Ankle Extensor Activity in Decerebrate Walking Cats. *J. Neurophysiol.* **92**, 2093–2104.

Dudley, R. (2018). *The Biomechanics of Insect Flight*. Princeton University Press.

Gorassini, M. A., Prochazka, A., Hiebert, G. W. and Gauthier, M. J. (1994). Corrective responses to loss of ground support during walking. I. Intact cats. *J. Neurophysiol.* **71**, 603–610.

Gould, S. J. and Vrba, E. S. (1982). Exaptation - a Missing Term in the Science of Form. *Paleobiology* **8**(1): 4–15.

Gunnell, G. F. and Simmons, N. B. (2012). *Evolutionary History of Bats*. Cambridge University Press.

Håkansson, J., Hedenström, A., Winter, Y. and Johansson, L. C. (2015). The wake of hovering flight in bats. *J. R. Soc. Interface.* **12**, 20150357–9.

Hedrick, T. L., Cheng, B. and Deng, X. (2009). Wingbeat time and the scaling of passive rotational damping in flapping flight. *Science.* **324**, 252–255.

Hermanson, J. W. and Altenbach, J. S. (1985). Functional anatomy of the shoulder and arm of the fruit-eating bat *Artibeus jamaicensis*. *J. Zool.* **205**, 157–177.

Hiebert, G. W., Gorassini, M. A., Jiang, W., Prochazka, A. and Pearson, K. G. (1994). Corrective responses to loss of ground support during walking. II. Comparison of intact and chronic spinal cats. *J. Neurophysiol.* **71**, 611–622.

Hothorn, T., Bretz, F. and Westfall, P. (2008). Simultaneous Inference in General Parametric Models. *Biom. J.* **50**, 346–363.

Hubel, T. Y., Hristov, N. I., Swartz, S. M. and Breuer, K. S. (2016). Wake structure and kinematics in two insectivorous bats. *Philos. Trans. R. Soc. Lond., B, Biol. Sci.* **371**, 20150385–12.

Iriarte-Diaz, J., Riskin, D. K., Willis, D. J., Breuer, K. S. and Swartz, S. M. (2011). Whole-body kinematics of a fruit bat reveal the influence of wing inertia on body accelerations. *J. Exp. Biol.* **214**, 1546–1553.

Jindrich, D. L. and Full, R. J. (2002). Dynamic stabilization of rapid hexapedal locomotion. *J. Exp. Biol.* **205**, 2803–2823.

Knörlein, B. J., Baier, D. B., Gatesy, S. M., Laurence-Chasen, J. D. and Brainerd, E. L. (2016). Validation of XMALab software for marker-based XROMM. *J. Exp. Biol.* **219**, 3701–3711.

Konow, N., Cheney, J. A., Roberts, T. J., Iriarte-Diaz, J., Breuer, K. S., Waldman, J. R. S. and Swartz, S. M. (2017). Speed-dependent modulation of wing muscle recruitment intensity and kinematics in two bat species. *J. Exp. Biol.* **220**, 1820–1829.

Konow, N., Cheney, J. A., Roberts, T. J., Waldman, J. R. S. and Swartz, S. M. (2015). Spring or string: does tendon elastic action influence wing muscle mechanics in bat flight? *Proc. R. Soc. Lond. B. Biol. Sci.* **282**, 20151832–7.

Kruyt, J. W., Quicazan-Rubio, E. M., van Heijst, G. F., Altshuler, D. L. and Lentink, D. (2014). Hummingbird wing efficacy depends on aspect ratio and compares with helicopter rotors. *J. R. Soc. Interface.* **11**, 20140585–20140585.

Nishikawa, K., Biewener, A. A., Aerts, P., Ahn, A. N., Chiel, H. J., Daley, M. A., Daniel, T. L., Full, R. J., Hale, M. E., Hedrick, T. L., et al. (2007). Neuromechanics: an integrative approach for understanding motor control. *Integr. Comp. Biol.* **47**, 16–54.

Ortega-Jimenez, V. M., Sapir, N., Wolf, M., Variano, E. A. and Dudley, R. (2014). Into turbulent air: size-dependent effects of von Karman vortex streets on hummingbird flight kinematics and energetics. *Proc. R. Soc. Lond. B. Biol. Sci.* **281**, 20140180–20140180.

R Core Team (2018). *R: A language and environment for statistical computing*. Vienna, Austria.

Ravi, S., Crall, J. D., McNeilly, L., Gagliardi, S. F., Biewener, A. A. and Combes, S. A. (2015). Hummingbird flight stability and control in freestream turbulent winds. *J. Exp. Biol.* **218**, 1444–1452.

Riskin, D. K., Bahlman, J. W., Hubel, T. Y., Ratcliffe, J. M., Kunz, T. H. and Swartz, S. M. (2009). Bats go head-under-heels: the biomechanics of landing on a ceiling. *J. Exp. Biol.* **212**, 945–953.

Riskin, D. K., Bergou, A., Breuer, K. S. and Swartz, S. M. (2012). Upstroke wing flexion and the inertial cost of bat flight. *Proc. R. Soc. Lond. B. Biol. Sci.* **279**, 2945–2950.

Riskin, D. K., Iriarte-Diaz, J., Middleton, K. M., Breuer, K. S. and Swartz, S. M. (2010). The effect of body size on the wing movements of pteropodid bats, with insights into thrust and lift production. *J. Exp. Biol.* **213**, 4110–4122.

Riskin, D. K., Willis, D. J., Iriarte-Diaz, J., Hedrick, T. L., Kostandov, M., Chen, J., Laidlaw, D. H., Breuer, K. S. and Swartz, S. M. (2008). Quantifying the complexity of bat wing kinematics. *J. Theor. Biol.* **254**, 604–615.

Ristroph, L., Bergou, A. J., Ristroph, G., Coumes, K., Berman, G. J., Guckenheimer, J., Wang, Z. J. and Cohen, I. (2010). Discovering the flight autostabilizer of fruit flies by inducing aerial stumbles. *Proc. Natl. Acad. Sci. U.S.A.* **107**, 4820–4824.

Roberts, T. J. and Azizi, E. (2011). Flexible Mechanisms: the Diverse Roles of Biological Springs in Vertebrate Movement. *J. Exp. Biol.* **214**, 353–361.

Simmons, N. B., Seymour, K. L., Habersetzer, J. and Gunnell, G. F. (2008). Primitive Early Eocene bat from Wyoming and the evolution of flight and echolocation. *Nature.* **451**, 818–821.

Sponberg, S. and Full, R. J. (2008). Neuromechanical response of musculo-skeletal structures in cockroaches during rapid running on rough terrain. *J. Exp. Biol.* **211**, 433–446.

Stengel, R. F. (2015). *Flight Dynamics*. Princeton University Press.

Sun, M., Wang, J. and Xiong, Y. (2007). Dynamic flight stability of hovering insects. *Acta. Mech. Sin.* **23**, 231–246.

Swartz, S. M. (1997). Allometric patterning in the limb skeleton of bats: Implications for the mechanics and energetics of powered flight. *J. Morphol.* **234**, 277–294.

Swartz, S. M. and Middleton, K. M. (2008). Biomechanics of the Bat Limb Skeleton: Scaling, Material Properties and Mechanics. *Cells Tissues Organs.* **187**, 59–84.

Vance, J. T., Faruque, I. and Humbert, J. S. (2013). Kinematic strategies for mitigating gust perturbations in insects. *Bioinspir. Biomim.* **8**, 016004.

Vaughan, T. A. (1959). Functional Morphology of Three Bats: *Eumops*, *Myotis*, *Macrotis*. *University of Kansas Publications.* **12**, 1–461.

Vaughan, T. A. (1970a). The Skeletal System. In *Biology of Bats* (ed. Wimsatt, W. A., pp. 98–139. New York, NY: Academic Press.

Vaughan, T. A. (1970b). The Muscular System. In *Biology of Bats* (ed. Wimsatt, W. A., pp. 140–194. New York, NY.

Vejdani, H. R., Boerma, D. B., Swartz, S. M. and Breuer, K. S. (2019). The dynamics of hovering flight in hummingbirds, insects and bats with implications for aerial robotics. *Bioinspir. Biomim.* **14**, 016003–18.

Vejdani, H., Boerma, D., Swartz, S. M. and Breuer, K. S. (2017). Guidelines for the design and control of bio-inspired hovering robots. pp. 4160–4166. IEEE.

Walton, D. W. and Walton, G. M. (1970). Post-cranial osteology of bats. In *About Bats: A Chiropteran Biology Symposium* (eds. Slaughter, B. H. and Walton, D. W.), pp. 93–128. Dallas: sites.smu.edu.

Warrick, D. R., Tobalske, B. W. and Powers, D. R. (2005). Aerodynamics of the hovering hummingbird. *Nature*. **435**, 1094–1097.

Weis-Fogh, T. (1973). Quick Estimates of Flight Fitness in Hovering Animals, Including Novel Mechanisms for Lift Production. *J. Exp. Biol.* **59**, 169–230.

Figure 1: Experimental design and perturbation experiments. (A) Frontal view of flight corridor partition, positioned at the midpoint of a 2 m x 2.2 m x 8.8 m corridor. Schematic indicates location of the aperture, perturbation apparatus, global coordinate system, and cameras. Sixth camera, which provides head-on view, not shown; (B) A representative roll-inducing wing perturbation followed by the recovery wingbeat, frontal view. Red arrow provides visual guide for the amount of body roll at each instance. Air jet is applying force to the wing in the first image. Images two and three show the recovery downstroke. Images four and five show the recovery upstroke; and (C) A representative pitch-inducing body perturbation followed by the recovery wingbeat, lateral view. Red arrow provides a visual guide for the amount of body pitch at each instance. Air jet is applying downward force to the caudal region of the body. Images two and three show the recovery upstroke. Images four and five show the recovery downstroke. All images were brightened and cropped so that the bat filled the full frame; no other digital modifications were applied.

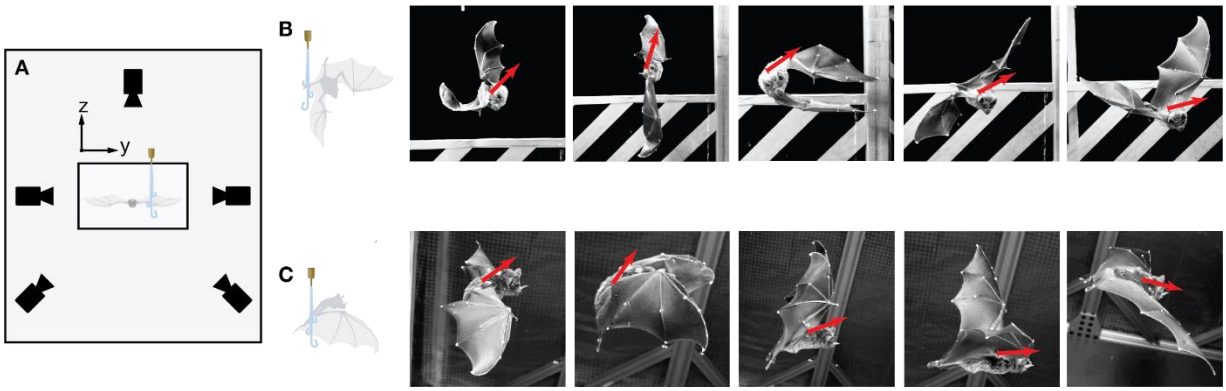

Figure 2: (A) Anatomical landmarks and (B) body-referenced coordinate system.

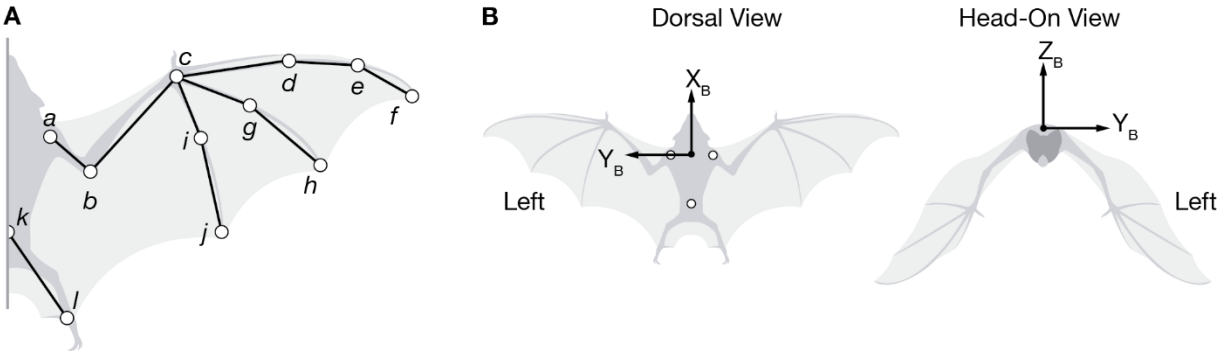

Figure 3: Kinematics for body perturbation recovery. (a-l, left column) Kinematic measurements following body perturbations (colored lines; six flights, mean ± 1 s.d., n=4 individuals) compared to control values (mean ± 1 s.d , black lines; four flights, n=2 individuals); and (c-m, right column) mean ± 1 s.d. values for left-right asymmetry (black lines designate control flights, green designate perturbed; mean ± 1 s.d.); zero indicates symmetrical wing movement. Grey shading indicates downstroke. Dashed vertical line denotes the end of the perturbation. Means shown here for clarity; raw data for individual trials provided in Fig. S3.

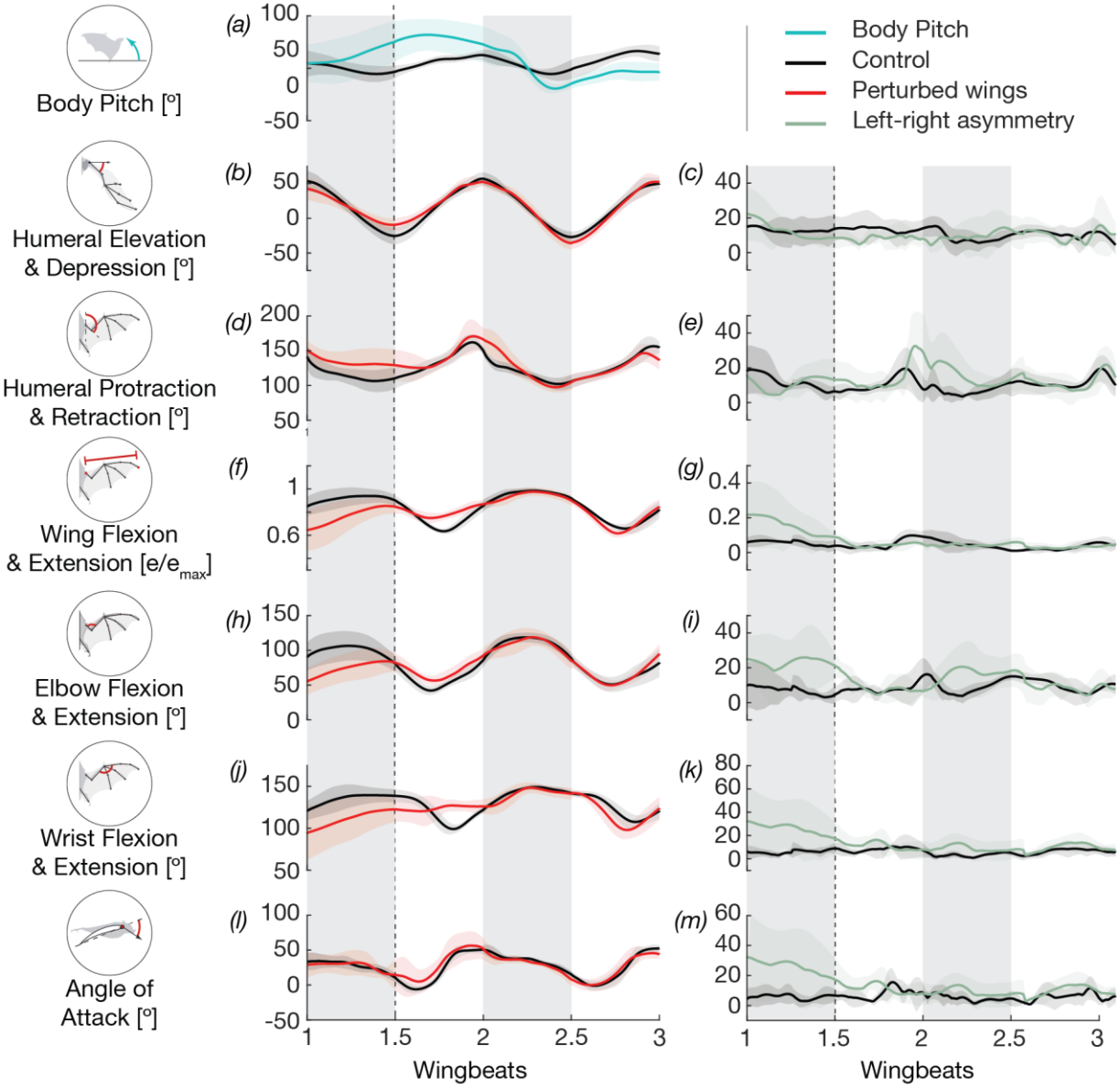

Figure 4: Kinematics for wing perturbation recovery. (a-l, left column) Kinematic measurements for wing perturbations (red and blue lines, mean ± 1 s.d. , five flights, n=2 individuals) compared to control values (black lines, mean ± 1 s.d; four flights, n=2 individuals). Red lines show values for wings on the perturbed side, and blue lines show values for wings on the unperturbed side; (c-m, right column) values for left-right asymmetry, with zero indicating symmetrical wing movements (black lines designate control flights, green designate perturbed; mean ± 1 s.d.). Grey bars indicate downstroke. Dashed vertical line denotes the end of the perturbation. Means shown here for clarity; raw data for individual trials provided in Fig. S4.

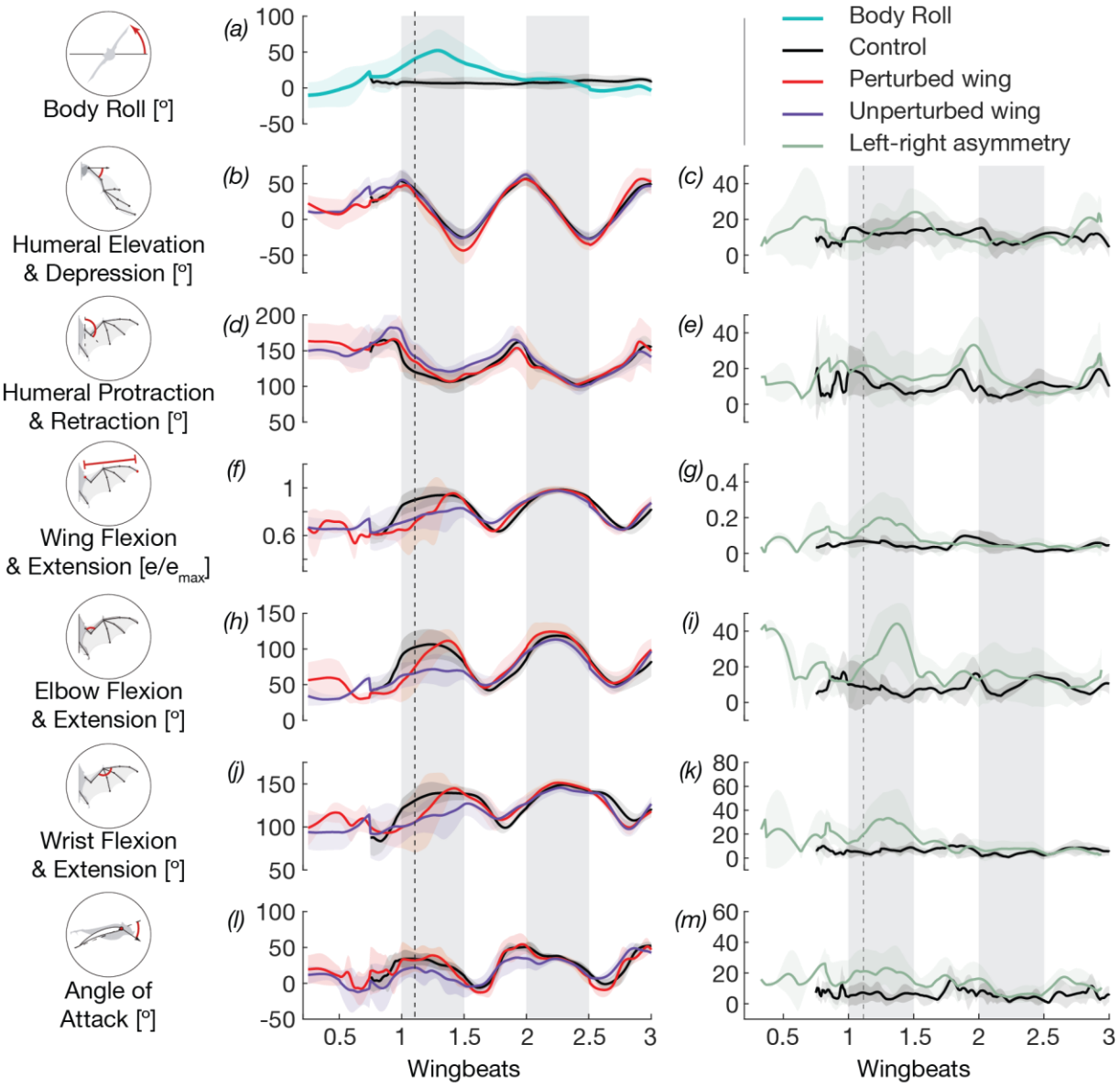

Figure 5: Changes in body roll predicted by the dynamical model from wing elevation/depression and flexion/extension alone. We performed two simulations using kinematics from two wing perturbation trials from the same individual: a slight perturbation resulting in 47° peak perturbed body roll orientation (*a*-*d*) and a severe perturbation resulting in 93° peak perturbed body roll orientation (*e*-*h*). Inputs were wing elevation/depression (*a* and *e*, left and right wings symmetrical in each), and total wing flexion/extension of left (blue) and right (red) wings, which was asymmetrical (*b* and *f*). From these inputs the model estimated changes in body roll angle resulting from inertial forces only (green) and from inertial plus aerodynamic forces (purple) (*c* and *g*). Dotted green and purple lines show roll angle near zero at the end of the recovery wingbeat. Estimated roll torques due to inertia (green), aerodynamics (blue), and inertia plus aerodynamics (purple, net roll torque) are shown in panels *d* and *h*, with positive values corresponding to torque that rotate the body opposite the direction imposed by the perturbation.

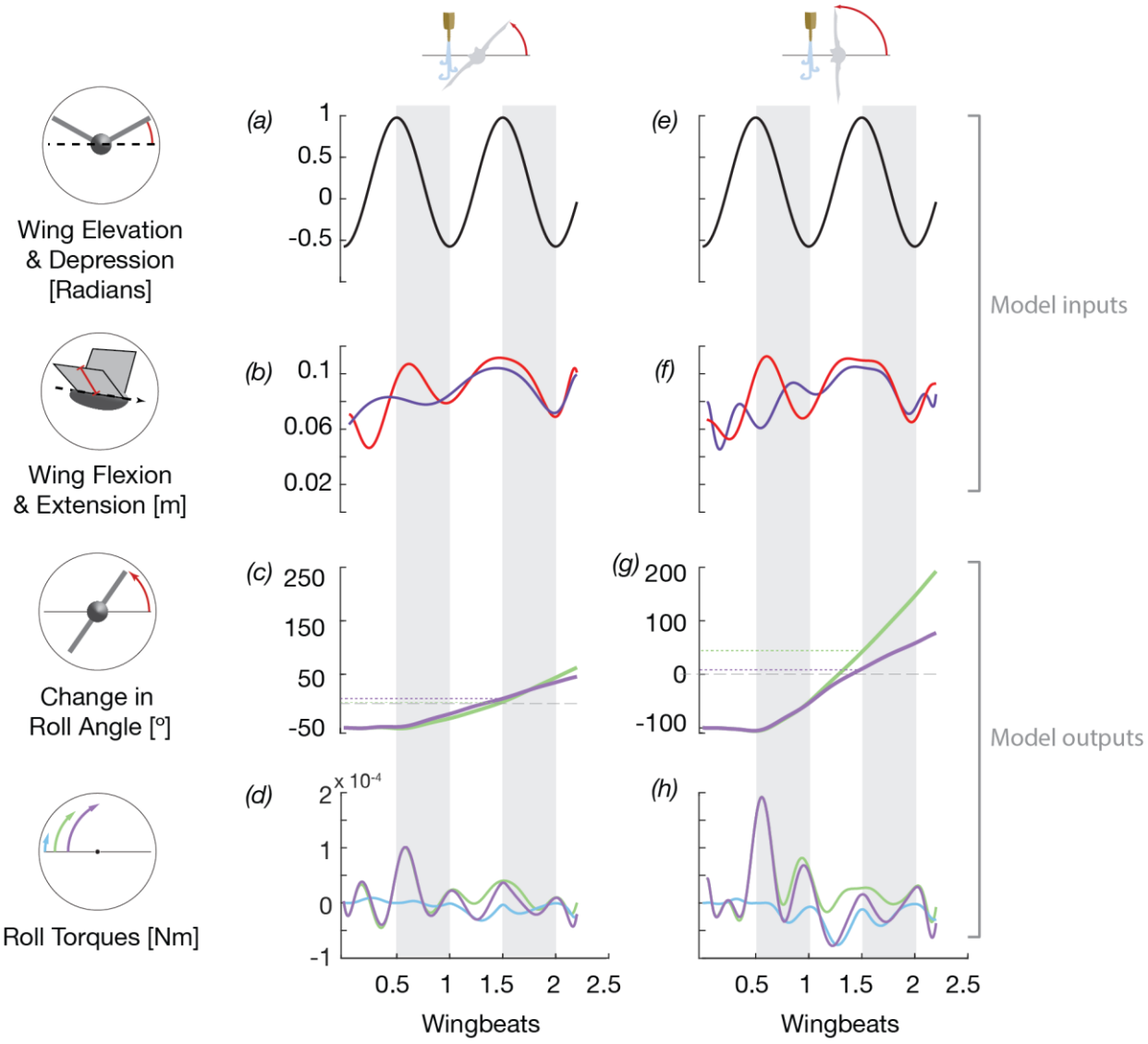

Table 1: Definitions of kinematic variables. All calculations refer to points shown in Figure 2.

Kinematic Variable	Calculation
Humeral elevation/depression	Angle of *a*-*b* in the Y_B-Z_B plane, relative to Y_B
Humeral protraction/retraction	Angle of *a*-*b* in the X_B-Y_B plane, relative to X_B
Wing extension/retraction	Distance *a*-*f*
Elbow flexion/extension	Angle *a*-*b*-*c*
Wrist flexion/extension	Angle *b*-*c*-*d*
Angle of attack	In the global coordinate system, angle of plane *a*-*c*-*j* relative to wrist velocity

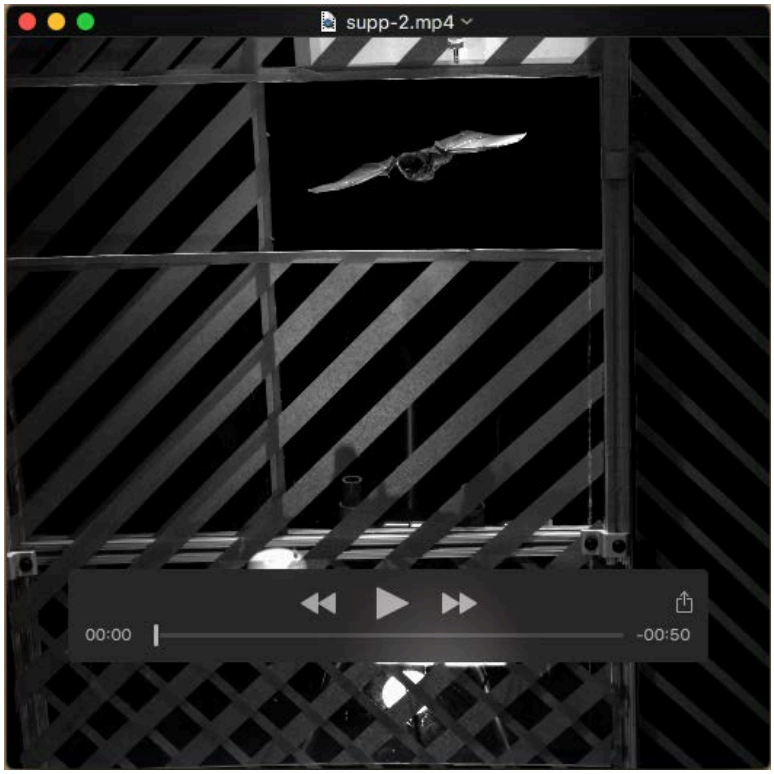

Movie 1: Unperturbed flight movie. Bat flying through the partition window without the perturbation jet.

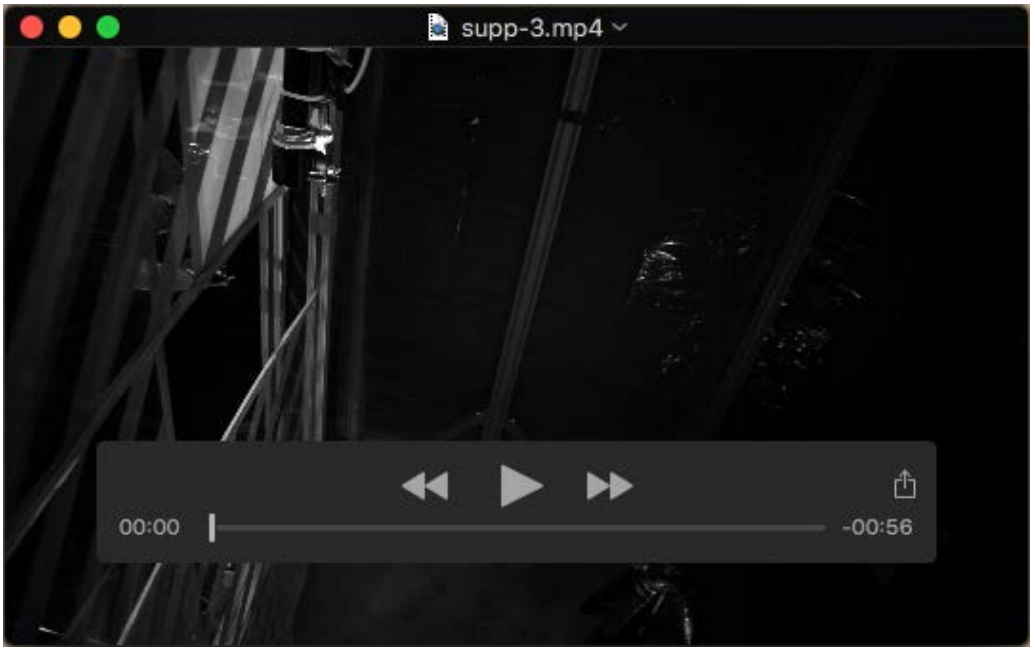

Movie 2: Body perturbation movie. Lateral view of bat experiencing and recovering from a pitch-inducing body perturbation.

Movie 3: Wing perturbation movie. Head-on view of a bat experiencing and recovering from a roll-inducing wing perturbation.

Figure S1: Gust perturbation characterization. Force profiles of gust perturbation at 5 cm (black), 7.5 cm (dark grey), and 10 cm (light grey). First two graphs show lateral forces (Fx and Fy); rightmost panel shows vertical force (Fz). Force is approximately 4.5 Newtons, more than twice the bodyweight of our study species, *Carollia perspicillata* (~18 g).

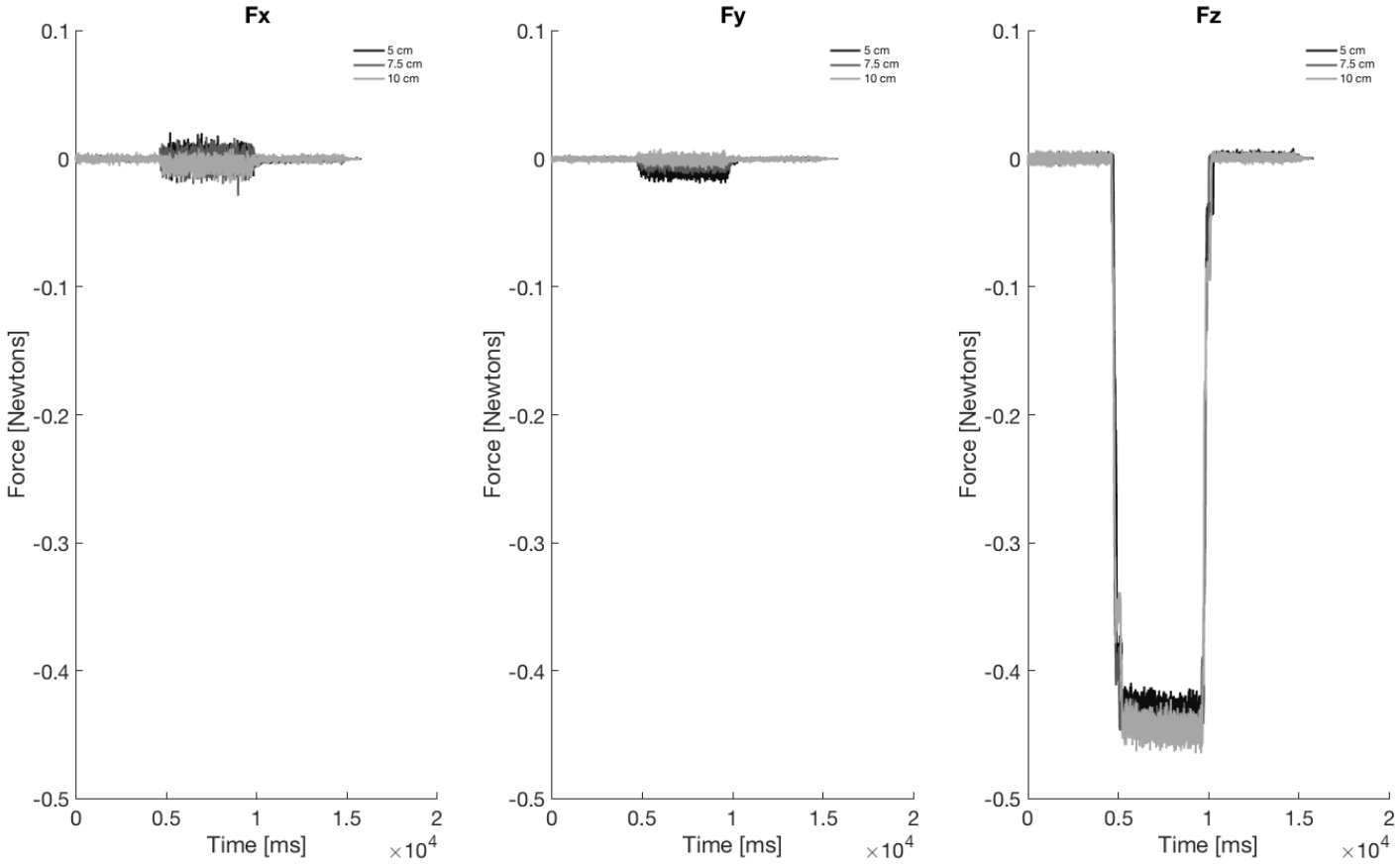

Figure S2: Unperturbed kinematics (left panels) and left right asymmetry (right panels) for each individual trial.

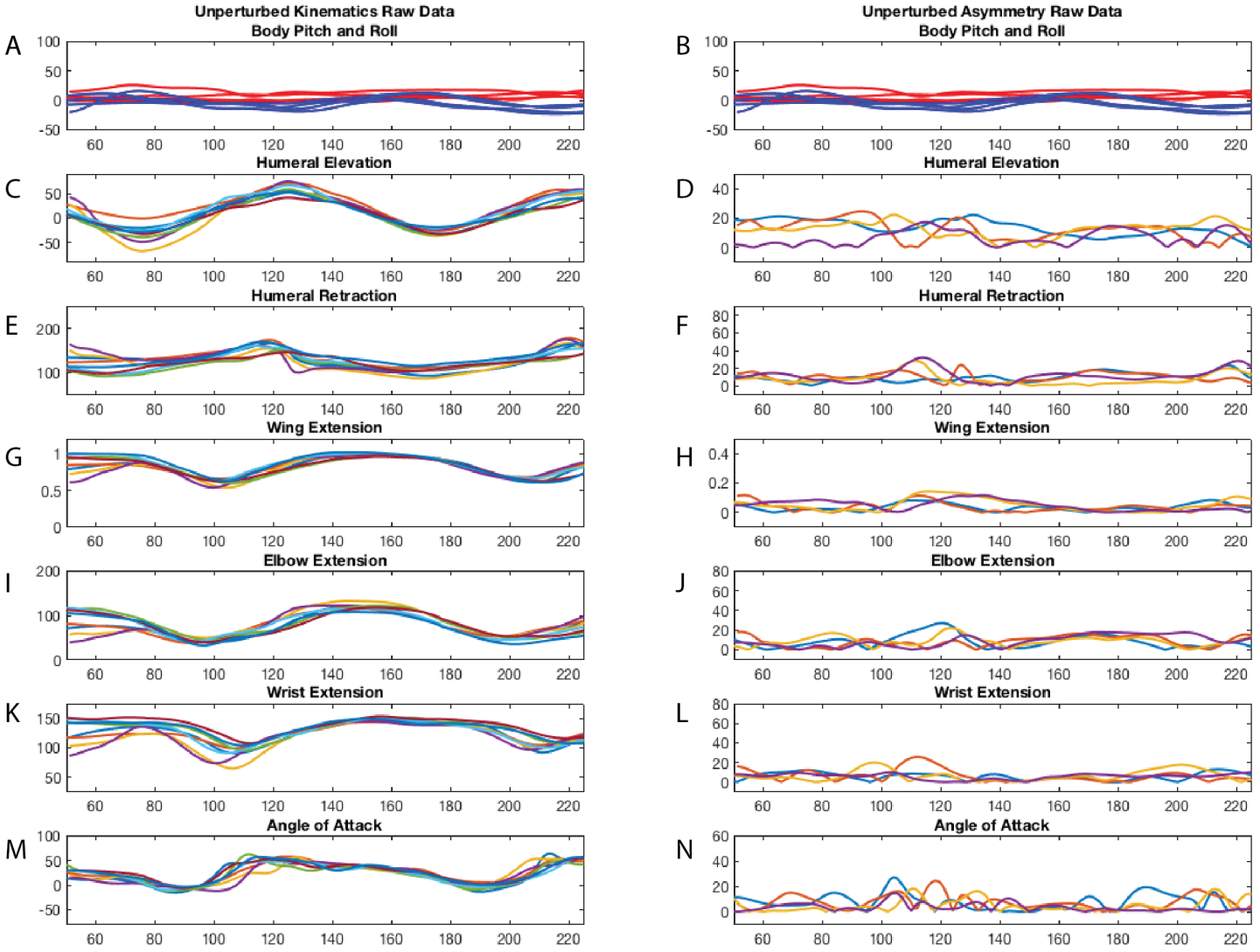

Figure S3: Body perturbation kinematics (left panels) and left right asymmetry (right panels) for each individual trial.

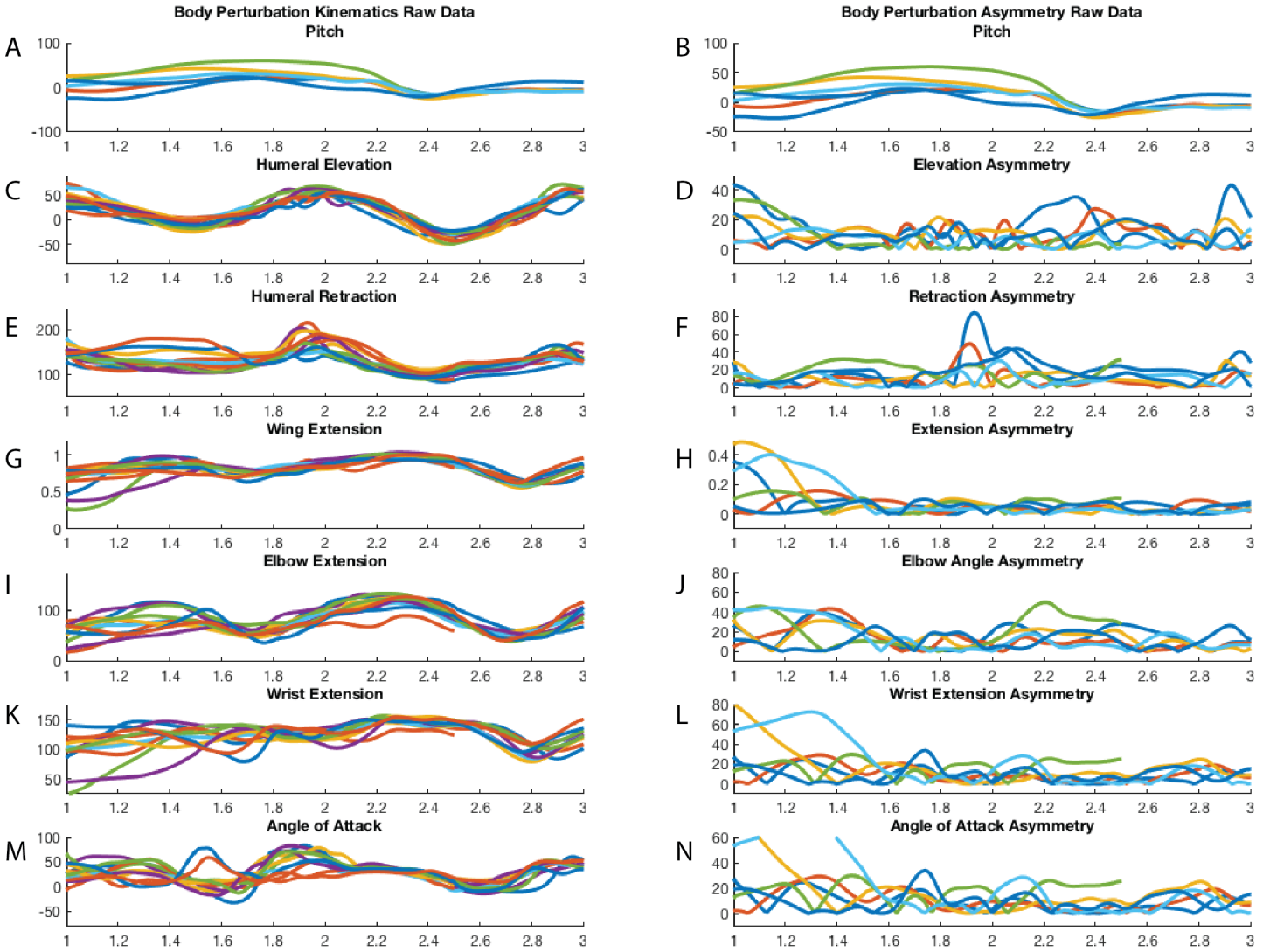

Figure S4: Wing perturbation kinematics (left panels) and left right asymmetry (right panels) for each individual trial.

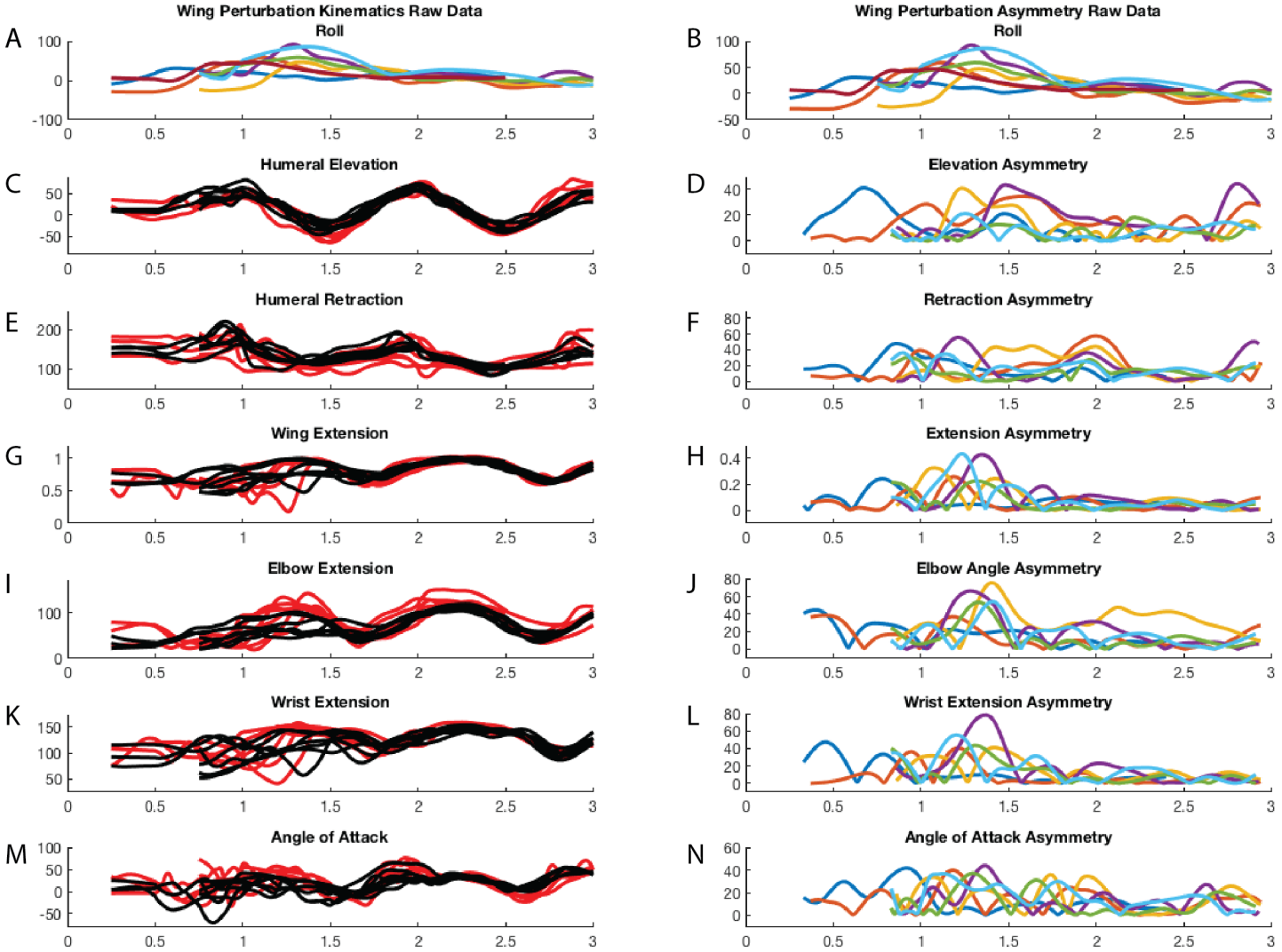

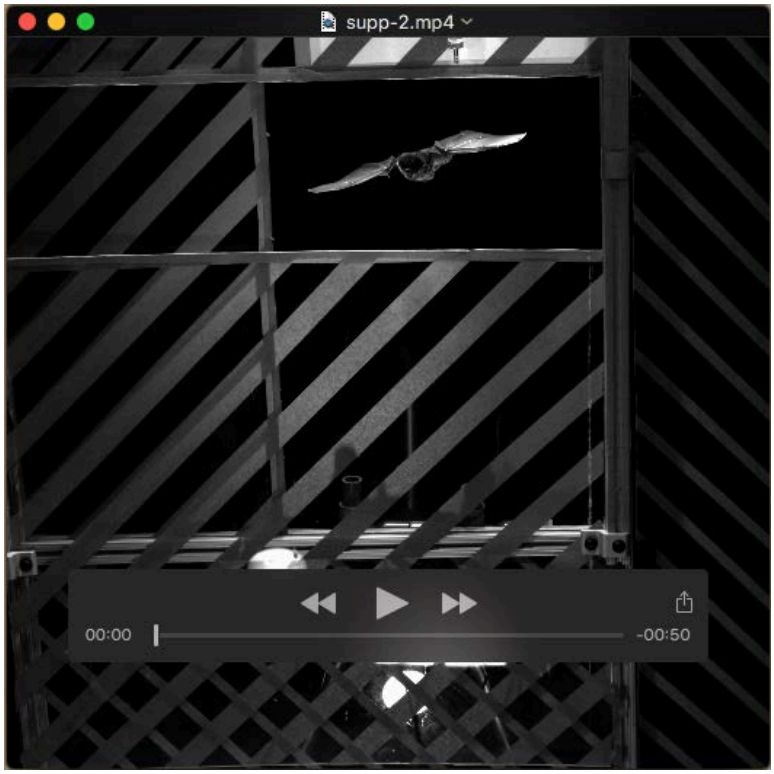

Movie 1: Unperturbed flight movie. Bat flying through the partition window without the perturbation jet.

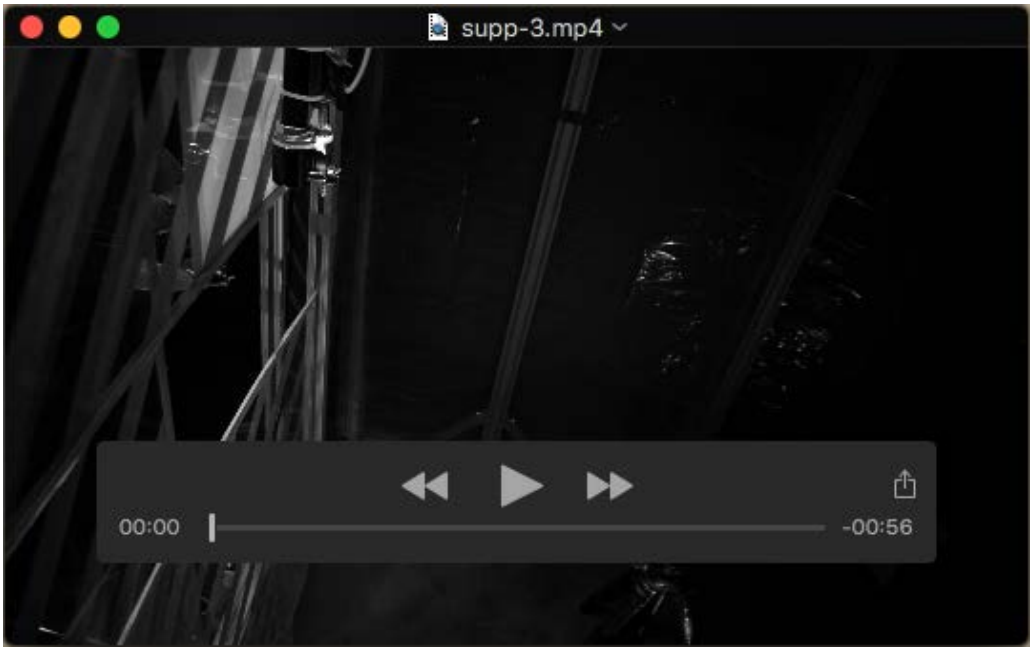

Movie 2: Body perturbation movie. Lateral view of bat experiencing and recovering from a pitch-inducing body perturbation.

Movie 3: Wing perturbation movie. Head-on view of a bat experiencing and recovering from a roll-inducing wing perturbation.

Figure S1: Gust perturbation characterization. Force profiles of gust perturbation at 5 cm (black), 7.5 cm (dark grey), and 10 cm (light grey). First two graphs show lateral forces (Fx and Fy); rightmost panel shows vertical force (Fz). Force is approximately 4.5 Newtons, more than twice the bodyweight of our study species, *Carollia perspicillata* (~18 g).

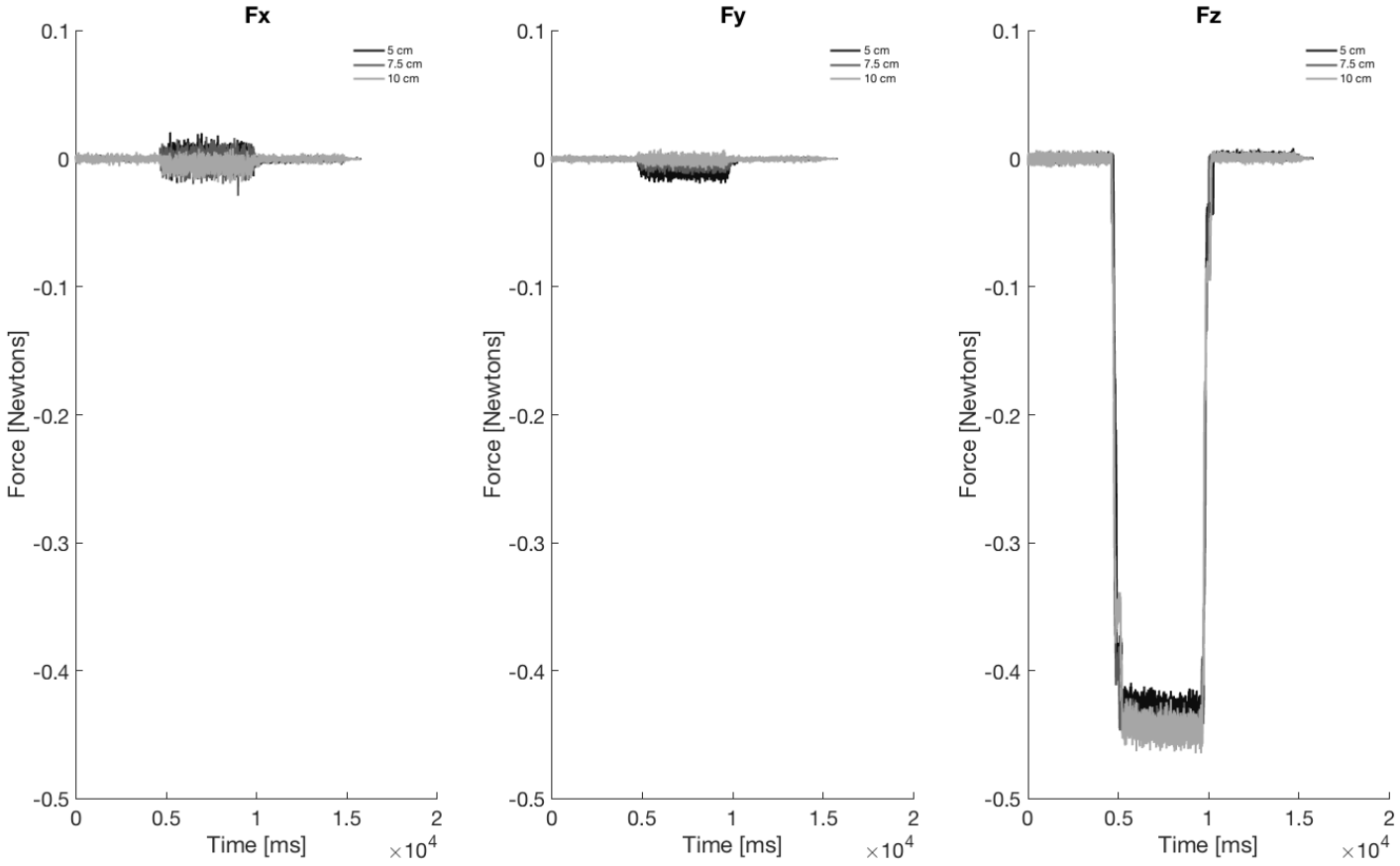

Figure S2: Unperturbed kinematics (left panels) and left right asymmetry (right panels) for each individual trial.

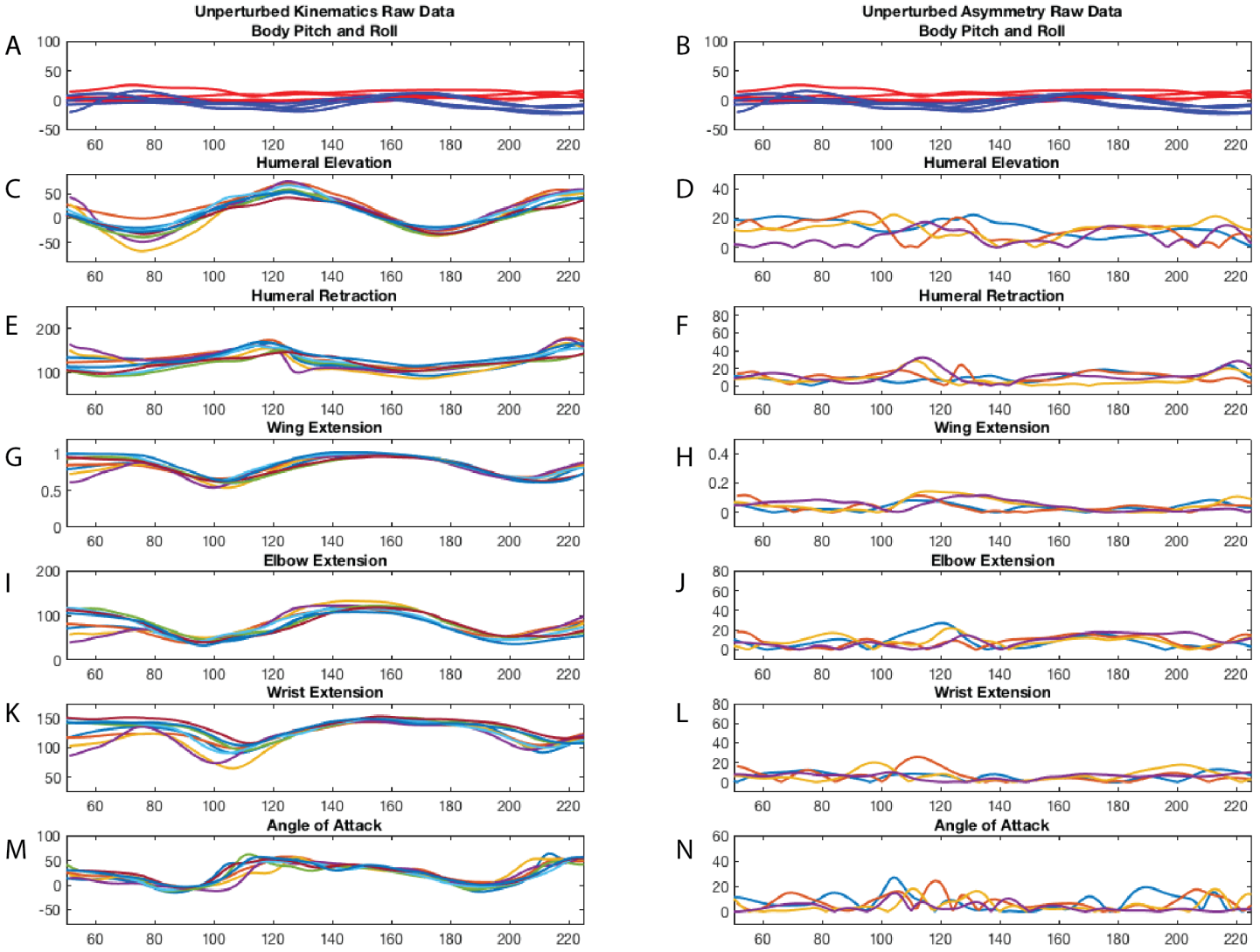

Figure S3: Body perturbation kinematics (left panels) and left right asymmetry (right panels) for each individual trial.

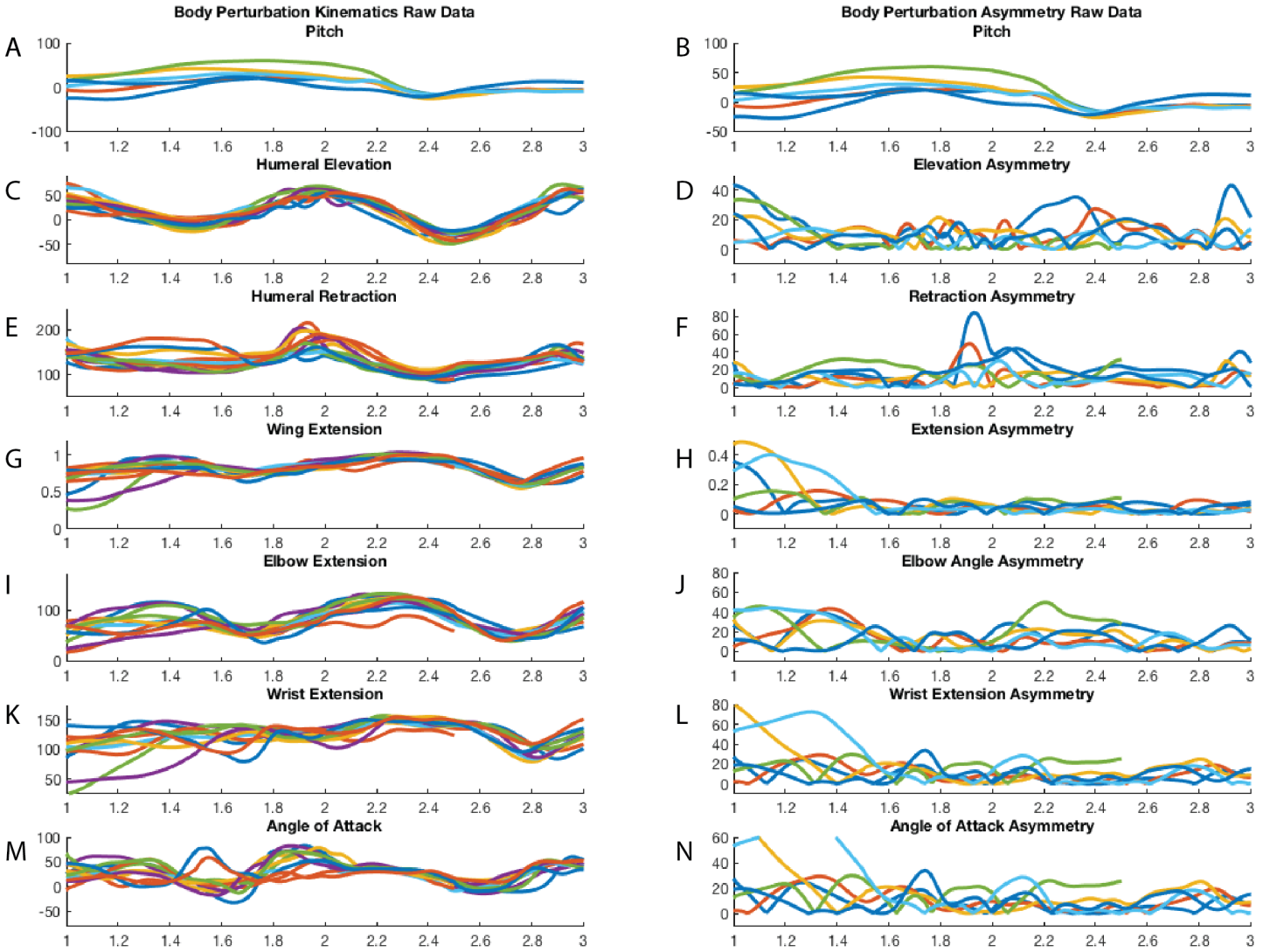

Figure S4: Wing perturbation kinematics (left panels) and left right asymmetry (right panels) for each individual trial.